Discover Oncology

RESEARCH Open Access

Spatial transcriptomic landscape and cellular neighborhood heterogeneity in cervical cancer: integrative single-cell and spatial RNA sequencing analysis

Dieyi Mo[1], Huana Cao[1], Shaojuan Lai[1], Jinding Luo[1] and Weijie Ye[2*]

*Correspondence:
Weijie Ye
ye206@163.com
[1]Department of Anesthesiology, Guangzhou Panyu Maternal And Child Health Care Hospital (He Xian Memorial Affiliated Hospital), Guangzhou 511400, China
[2]Department of Respiratory, Guangzhou Panyu Maternal And Child Health Care Hospital (He Xian Memorial Affiliated Hospital), Guangzhou 511400, China

Abstract

Background Cervical cancer ranks as the fourth most common malignancy among women worldwide, with approximately 604,000 new cases and 342,000 deaths annually. Despite advances in HPV vaccination and screening programs, significant challenges remain in diagnostic accuracy, therapeutic efficacy, and prognostic assessment. Traditional bulk RNA sequencing methods average gene expression data across entire tissue specimens, masking cellular diversity and spatial architectural patterns that influence tumor progression. Telomere maintenance mechanisms play crucial roles in cervical cancer development, with over 90% of cervical cancers exhibiting telomerase reactivation.

Methods This study integrated single-cell RNA sequencing and spatial transcriptomics technologies to construct the first comprehensive spatial molecular atlas of cervical cancer. Single-cell RNA sequencing analysis utilized public datasets from the GEO database with systematic quality control through a multidimensional assessment framework. Spatial transcriptomics analysis employed the 10x Genomics Visium platform, successfully identifying 38 distinct cellular neighborhoods (N1-N38). Spatial expression patterns of 10 key genes were analyzed, including epithelial markers (MUC1, CDH1, KRT16), stromal markers (COL1A1, COMP, DCN), and immune markers (CD3G, FCGR1A). In vitro validation was performed using HeLa and SiHa cell lines.

Results Multiple distinct cell subpopulations and 38 cellular neighborhoods with unique molecular characteristics were successfully identified. MKI67 demonstrated spatial heterogeneity with proliferative "hotspots"; COMP was primarily expressed in stromal regions and participated in tumor-stroma interactions; KRT16 exhibited patterns reflecting epithelial differentiation gradients. Different neighborhoods showed enrichment for various cell types, including immune hotspots, stromal-rich regions, and epithelial-dominant areas. Immunoglobulin-related genes (IGLC2, IGHG1, IGHG2, etc.) displayed unique spatial expression characteristics. Quantitative PCR validation confirmed differential expression patterns between cell lines.

Conclusions This study established the first comprehensive spatial transcriptomic atlas of cervical cancer, revealing unprecedented insights into tumor microenvironment organization and cellular spatial relationships.

Keywords Spatial transcriptomics, Single-cell RNA sequencing, Cervical cancer, Tumor microenvironment, Cellular neighborhoods, Gene expression heterogeneity

1 Introduction

Among women worldwide, cervical cancer ranks as the fourth most prevalent malignancy, contributing to approximately 604,000 new diagnoses and 342,000 fatalities each year. While human papillomavirus (HPV) vaccination programs and enhanced screening initiatives have yielded considerable preventive advances, significant obstacles remain in diagnostic accuracy, therapeutic efficacy, and prognostic assessment—challenges that are particularly pronounced in resource-constrained environments [1–3]. The tumor microenvironment (TME) in cervical cancer demonstrates remarkable heterogeneity, characterized by intricate interactions among malignant epithelial cells, stromal elements, and diverse immune cell populations.

Bulk RNA sequencing methodologies, while widely utilized, generate averaged gene expression data across complete tissue specimens, thereby obscuring essential cellular diversity and spatial architectural patterns that fundamentally influence tumor advancement and resistance to therapeutic interventions. This averaging effect masks the complex cellular ecosystems that exist within tumors and limits our understanding of the mechanisms driving disease progression. The emergence of single-cell RNA sequencing (scRNA-seq) technology has fundamentally transformed tumor biology comprehension by enabling detailed characterization of cellular diversity within malignant tissues. This technological advancement facilitates the discovery of rare cellular subpopulations, elucidation of developmental pathways, and mapping of intercellular communication networks [4, 5]. Nevertheless, the tissue dissociation process inherent to scRNA-seq methodology results in the inevitable loss of crucial spatial contextual information.

The field of transcriptomic analysis has experienced a paradigm transformation through spatial transcriptomics technology, which permits concurrent assessment of gene expression profiles and spatial positioning within preserved tissue architecture. This innovative approach successfully bridges the analytical gap between single-cell precision and spatial context preservation, offering unparalleled insights into the contributions of cellular interactions and spatial organization to disease development [6–8]. Contemporary cancer research applications of spatial transcriptomics have successfully revealed spatial gene expression gradients, characterized tumor-immune boundary dynamics, and identified therapeutically relevant targets with spatial restrictions.

Cervical cancer development and progression are significantly influenced by telomere maintenance mechanisms. More than 90% of cervical cancers exhibit telomerase reactivation, which facilitates unlimited cellular replicative capacity while contributing to genomic instability [9, 10]. Critical telomere maintenance genes demonstrate altered expression profiles in cervical cancer, including MKI67 (serving as a proliferation indicator), COMP (cartilage oligomeric matrix protein), and multiple keratin variants. Spatial distribution analysis of these genes within tumor tissues offers potential insights into proliferative regions and cellular differentiation gradients.

The cervical cancer immune microenvironment exhibits exceptional complexity, encompassing diverse immune cell populations that demonstrate distinct spatial distributions and functional characteristics. Humoral immune responses involve immunoglobulin-producing plasma cells and B cells, whose spatial positioning relative to malignant cells may significantly impact therapeutic response rates [11–13]. Understanding immune surveillance and evasion mechanisms requires comprehensive spatial analysis of immune-related genes, including immunoglobulin chains (IGLC2, IGHG1, IGHG2, IGLC3, IGHG3, IGKC) and immune cell markers (CD3G, FCGR1A).

Our investigation represents the first comprehensive spatial molecular atlas construction for cervical cancer through the integration of single-cell RNA sequencing and spatial transcriptomics technologies. The research objectives encompassed five primary aims: (1) cellular heterogeneity characterization and distinct cell population identification within cervical cancer tissues; (2) spatial gene expression pattern mapping for key molecular indicators; (3) cellular neighborhood identification featuring unique spatial organization and functional properties; (4) telomere maintenance gene expression pattern investigation across various cell types and spatial regions; and (5) immune-related gene spatial distribution analysis for understanding tumor-immune interactions.

2 Methods

2.1 Single-Cell RNA sequencing

The transcriptomic profiling of cervical cancer tissue samples was achieved through comprehensive single-cell RNA sequencing analysis. Public datasets from the Gene Expression Omnibus (GEO) database served as the primary data source, with raw single-cell RNA sequencing information extracted from multiple GEO accessions containing cervical cancer specimens [14, 15]. A multidimensional quality assessment framework formed the foundation of systematic quality control procedures. Four primary evaluation parameters guided this assessment: transcriptional activity measurement through total RNA counts per cell (nCount_RNA), detection sensitivity evaluation via the number of detected gene features (nFeature_RNA), cell viability assessment using mitochondrial gene expression proportions (percent.mt) as stress and death indicators, and protein synthesis activity monitoring through ribosomal gene expression proportions (percent.ribo).Technical bias identification involved Pearson correlation analysis between mitochondrial gene counts and total RNA counts. Distribution pattern visualization utilized density plots and violin plots to establish appropriate filtering thresholds for quality control metrics. Two-dimensional distribution relationships between RNA counts and feature gene counts were displayed through heatmap visualization, facilitating the identification of high-quality cells suitable for downstream analysis.

2.2 Multidimensional analysis of telomerase maintenance genes

The investigation of telomere maintenance-related genes employed comprehensive multidimensional analytical strategies, with particular emphasis on molecular mechanisms governing cell proliferation and genomic stability. Key genes including MKI67, COMP, KRT16, and CCL24 were incorporated into expression profile heatmaps, revealing distinct differential expression patterns across various cell types.Notable expression profile variations emerged among cycling cells, fibroblasts, and squamous epithelial cells. Three-dimensional visualization approaches created telomere expression landscapes,

where cellular positioning in 3D space reflected telomerase activity-related gene expression levels, providing intuitive representation of spatial distribution and functional states within different cell subpopulations.Network analysis methodologies facilitated the construction of gene co-expression constellation networks, unveiling synergistic expression relationships and functional modules among telomere maintenance genes. An innovative approach involved converting gene expression levels into musical notation format, creating dynamic visualization of telomere gene expression patterns throughout cellular developmental timelines.

2.3 Weighted gene co-expression network analysis

The application of Weighted Gene Co-expression Network Analysis (WGCNA) enabled deep exploration of synergistic gene expression relationships through co-expression network construction. Initial soft threshold selection involved calculating topological network fit indices and average connectivity across different threshold values, ultimately identifying optimal soft thresholds that enable scale-free topological network characteristics [16–18]. Construction of gene adjacency matrices and topological overlap matrices preceded hierarchical clustering approaches for co-expressed gene module identification. Specific cell type analysis, particularly focusing on neutrophils, utilized hdWGCNA methodology with dynamic tree cutting techniques to identify functional gene modules, establishing minimum module sizes of 30 genes.Module eigengene correlation analysis with cellular phenotypes revealed key gene modules associated with specific biological functions. The biological significance of identified modules underwent validation through Gene Ontology and KEGG pathway enrichment analyses.

2.4 Spatial transcriptomics analysis

Fine-scale spatial analysis of cervical cancer tissues was accomplished using spatial transcriptomics technology, specifically employing the 10x Genomics Visium platform for spatial gene expression data acquisition. Tissue section preparation maintained 10 μm thickness to optimize morphological preservation while ensuring RNA quality standards.Spatial clustering algorithms successfully identified 38 distinct cellular neighborhoods (N1-N38), each characterized by spatial spots exhibiting similar gene expression patterns. Graph-based clustering methodologies constructed spatial neighborhood networks based on both spatial adjacency relationships and gene expression similarity measures.Unique cellular spatial distribution patterns and gene expression characteristics distinguished each neighborhood, with RGB color coding systems differentiating cell types or functional states within neighborhoods. Neighborhood-specific marker gene identification resulted from inter-neighborhood gene expression difference calculations. Spatial autocorrelation assessment utilized analysis methods that evaluated spatial clustering patterns of gene expression, with Moran's I index providing quantitative measures of spatial autocorrelation degrees.Quality control procedures for spatial transcriptomics data established spatial-specific assessment standards. Gene count distribution (nCount_Spatial) and detected gene feature distribution (nFeature_Spatial) evaluation for each spatial spot reflected transcriptional activity and gene detection sensitivity. Color gradient heatmaps provided visualization of high-quality spatial spot distributions, enabling identification of specific tissue regions and spatial heterogeneity patterns. Spatial consistency assessment involved calculating spatial spot density and spatial

variation coefficients of gene expression. Morphology-guided quality control approaches integrated H&E staining image information to filter low-quality spatial spots positioned at tissue edges or within artifact regions.

2.5 Multi-gene spatial expression patterns

The construction of multi-gene spatial expression profiles involved systematic analysis of spatial expression distribution patterns for 10 key genes within cervical cancer tissues. Gene selection encompassed diverse cell types and functional categories: epithelial cell identification relied on markers including MUC1, CDH1, and KRT16, which demonstrated high expression primarily in tumor cell-enriched regions; stromal area characterization utilized connective tissue-related genes such as COL1A1, COMP, and DCN, showing strong expression signals in stromal regions; immune cell infiltration detection employed markers including CD3G and FCGR1A, displaying elevated expression in immune cell infiltration areas; specific cell subpopulation identification utilized transcriptional regulator GATA3; tissue remodeling-active region characterization relied on protease gene TMPRSS11E expression.Continuous spatial expression map construction utilized spatial interpolation algorithms for predicting gene expression levels in unsampled regions. Expression boundary and transition zone identification involved calculating spatial gradients of gene expression.

2.6 Immune-related gene spatial distribution

Special focus was directed toward spatial expression patterns of immunoglobulin-related genes, including IGLC2, IGHG1, IGHG2, IGLC3, IGHG3, and IGKC, which show primary expression in B cells and plasma cells. Spatial co-localization analysis investigated expression relationships among different immunoglobulin genes within spatial contexts. Tissue division into tumor regions, stromal regions, and immune infiltration regions was achieved through spatial domain decomposition methods, enabling analysis of immune gene expression characteristics within each defined region. Immune cell spatial distribution pattern quantification utilized spatial clustering indices of immune gene expression. Immune microenvironment spatial mapping identified both immune hotspot regions and immune desert areas.

2.7 Cell culture and maintenance

HeLa (HPV18-positive adenocarcinoma) and SiHa (HPV16-positive squamous cell carcinoma) cervical cancer cell lines were obtained from the American Type Culture Collection (ATCC, Manassas, VA, USA). HeLa cells were cultured in Dulbecco's Modified Eagle Medium (DMEM; Gibco, Thermo Fisher Scientific) supplemented with 10% fetal bovine serum (FBS; Gibco) and 1% penicillin-streptomycin (Gibco). SiHa cells were maintained in Minimum Essential Medium (MEM; Gibco) containing 10% FBS and 1% penicillin-streptomycin. Both cell lines were incubated at 37 °C in a humidified atmosphere with 5% CO_2. Cells were subcultured every 2–3 days upon reaching 80–90% confluence using 0.25% trypsin-EDTA (Gibco).

2.8 Quantitative real-time PCR analysis

Total RNA was extracted from cultured cells using TRIzol reagent (Invitrogen) according to the manufacturer's protocol. RNA quality and concentration were assessed using

a NanoDrop 2000 spectrophotometer (Thermo Fisher Scientific). First-strand cDNA was synthesized from 1 μg of total RNA using the SuperScript III Reverse Transcriptase kit (Invitrogen) with random hexamer primers. Quantitative PCR was performed using SYBR Green PCR Master Mix (Applied Biosystems) on a QuantStudio 3 Real-Time PCR System (Applied Biosystems).Primer sequences used were as follows: MUC1 forward 5'-CGTCGTGGACATTGATGGTACC-3', reverse 5'-GGGCAGCAGTTGATGATGAA-3'; CDH1 forward 5'-CGAGAGCTACACGTTCACGG-3', reverse 5'-GGGTGTCGAGGGAAAAATAGG-3'; KRT16 forward 5'-CTCCAGGTCCGAGATGAACA-3', reverse 5'-GCTTCTGCCATTTGCAAGAT-3'; GAPDH forward 5'-GAGTCAACGGATTTGGTCGT-3', reverse 5'-TTGATTTTGGAGGGATCTCG-3'. PCR conditions included initial denaturation at 95 °C for 10 min, followed by 40 cycles of 95 °C for 15 s and 60 °C for 1 min. Relative gene expression was calculated using the 2^(-ΔΔCt) method with GAPDH as the internal control. Each experiment was performed in triplicate with three independent biological replicates.

2.9 Data visualization and statistical analysis

All analysis results were presented using appropriate visualization methods, employing multiple graphic types to enhance data readability and interpretability. Heatmaps displayed gene expression matrices and correlation analysis results, with hierarchical clustering applied to order rows and columns. Scatter plots showed quality control metrics and gene variability analyses, using color coding and point size encoding for multidimensional information. Dimensionality reduction projection plots (UMAP, t-SNE) visualized cell clustering results, using different colors to distinguish cell types. Spatial expression maps used color intensity encoding for gene expression levels, overlaid on tissue section images. Violin plots and box plots displayed gene expression distributions across different cell types. Data processing and statistical analysis were performed using R language (version 4.1.0) and related bioinformatics software packages, primarily including Seurat, Monocle, and WGCNA. Statistical significance testing employed Wilcoxon rank-sum tests and Fisher's exact tests, with multiple comparison correction using the Benjamini-Hochberg method and significance levels set at $p < 0.05$. All analysis codes and parameter settings were documented to ensure result reproducibility and transparency.

3 Results

3.1 Quality control and cell clustering analysis of single-cell RNA sequencing in cervical cancer

This figure presents a comprehensive analysis of single-cell RNA sequencing data from cervical cancer samples. Figure 1A displays quality control metrics correlation analysis, where red dots represent the relationship between mitochondrial gene counts and RNA counts, while teal dots show the distribution pattern of another set of quality control parameters, both exhibiting clear linear correlation trends. Figure 1B presents a heatmap analysis of the relationship between RNA counts and feature gene counts, with different color intensities reflecting the abundance distribution of gene expression, where orange and purple regions represent high and low expression areas, respectively. Figure 1C and D show cell clustering results based on UMAP and t-SNE algorithms, successfully identifying multiple distinct cell subpopulations, with each color representing a specific cell

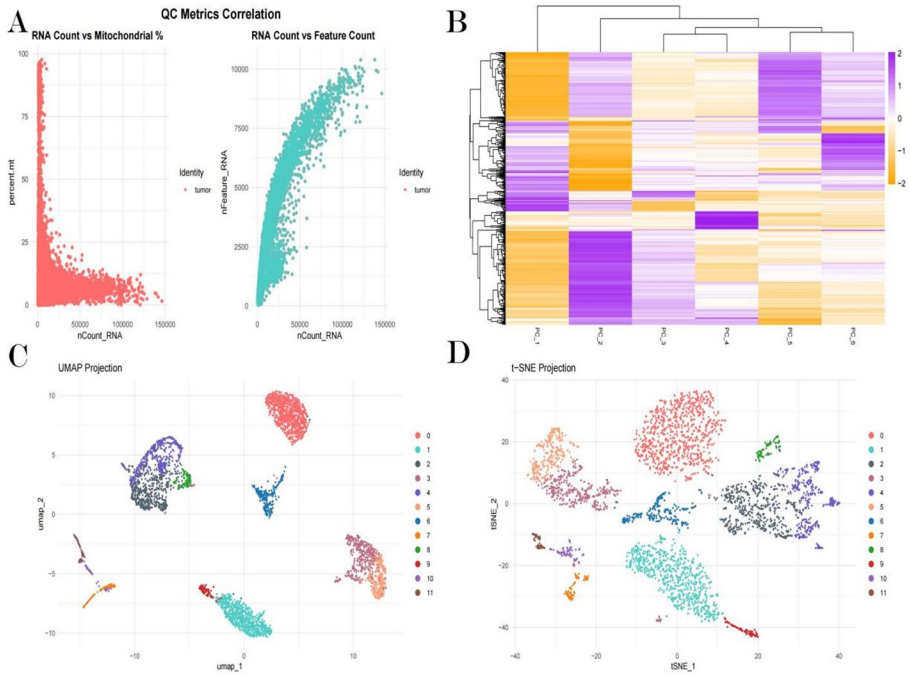

Fig. 1 Single-cell RNA sequencing quality control and clustering analysis of cervical cancer samples. (A) Quality control metrics correlation showing the relationship between mitochondrial gene counts and total RNA counts. (B) Heatmap visualization of RNA count versus feature count distribution. (C) UMAP-based dimensional reduction and cell clustering identification. (D) t-SNE projection displaying cellular heterogeneity and distinct cell populations. Different colors in panels C and D represent various cell types or functional states identified through unsupervised clustering analysis

type or functional state. These clustering results provide an important foundation for subsequent differential gene expression analysis and cell functional annotation.

3.2 Identification of hypervariable genes in single-cell transcriptome of cervical cancer and cell type annotation analysis

This figure demonstrates detailed analysis results of highly variable gene identification and cell type annotation in cervical cancer single-cell RNA sequencing data. Figure 2A shows highly variable gene analysis, identifying gene sets with significant expression differences between cells, where red scatter points represent selected highly variable genes that play crucial roles in subsequent dimensionality reduction analysis and cell clustering. Figure 2B presents JackStraw analysis results for determining the optimal number of principal components, with green solid lines indicating statistically significant principal components, providing scientific basis for dimensionality reduction analysis. Figure 2C and D respectively show cell type annotation results based on different parameter settings, successfully identifying multiple cell types including cycling cells, fibroblasts, epithelial cells, plasma cells, smooth muscle cells, and others. Each color represents a specific cell subpopulation, revealing the complex cellular heterogeneity and microenvironmental composition within cervical cancer tissues.

3.3 Multidimensional analysis of telomerase maintenance gene expression patterns in cervical cancer single-cell transcriptome

This figure presents a comprehensive multi-dimensional analysis of telomere maintenance gene expression patterns in cervical cancer single-cell RNA sequencing data.

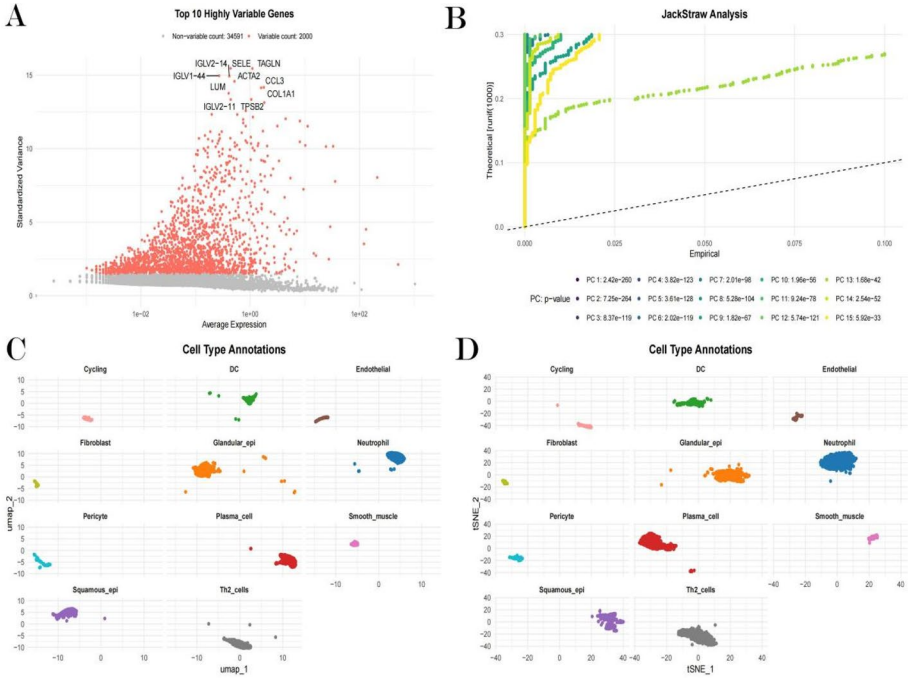

Fig. 2 Highly variable gene identification and cell type annotation in cervical cancer single-cell transcriptomics. (A) Highly variable gene analysis showing genes with significant expression variability across cells (red dots represent selected highly variable genes). (B) JackStraw analysis for principal component selection, with green lines indicating statistically significant components. (C, D) Cell type annotation results displaying distinct cellular populations including cycling cells, fibroblasts, epithelial cells, plasma cells, and smooth muscle cells. Different colors represent various annotated cell types, revealing the cellular diversity within the cervical cancer microenvironment

Figure 3A displays a heatmap showing the expression patterns of key telomere maintenance genes (MKI67, COMP, KRT16, CCL24, etc.) across different cell types, with cycling cells, fibroblasts, and squamous epithelial cells exhibiting distinct gene expression profiles. Figure 3B presents a three-dimensional landscape of telomere expression, visualizing the spatial distribution and telomerase activity states of different cell subpopulations. Figure 3C shows a constellation network diagram of telomere gene expression, revealing co-expression relationships and functional modules among genes. Figure 3D employs an innovative musical score visualization method, converting gene expression levels into musical notation format to intuitively demonstrate the dynamic expression patterns of telomere genes along the cellular developmental timeline. Panel E displays the soft threshold selection results for Weighted Gene Co-expression Network Analysis (WGCNA), providing optimal parameters for constructing gene co-expression networks. Panel F presents a dendrogram from neutrophil-specific WGCNA analysis, with the bottom color bar representing different gene functional modules, revealing the modular expression characteristics of telomere-related genes in neutrophils.

3.4 Single-cell transcriptomic analysis of gene expression patterns in cervical cancer

This study conducted comprehensive gene expression analysis of cervical cancer samples using single-cell RNA sequencing technology. Figure 4A displays the cellular organelle gene expression map, showing the expression distribution patterns of organelle-related genes through color-coded circular regions, revealing the heterogeneity of organelle functions in cervical cancer cells. Figure 4B presents the genome gene functional

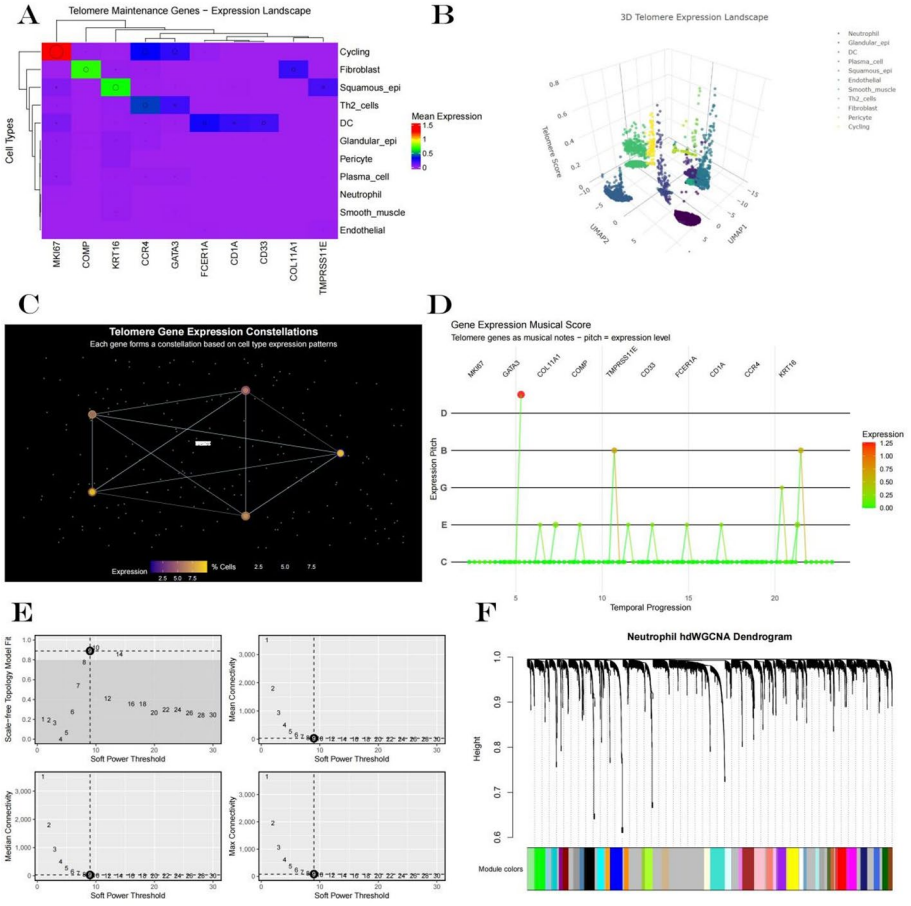

Fig. 3 Multi-dimensional analysis of telomere maintenance gene expression in cervical cancer single-cell transcriptomics. (A) Heatmap showing telomere maintenance gene expression across cell types. (B) 3D telomere expression landscape visualization. (C) Gene expression constellation network revealing co-expression patterns. (D) Musical score representation of gene expression dynamics over temporal progression. (E) WGCNA soft threshold selection plots showing scale-free topology model fit and mean connectivity. (F) Neutrophil hdWGCNA dendrogram with module color assignments showing gene clustering patterns and functional modules

landscape, utilizing dimensionality reduction analysis to cluster genes according to their functional characteristics, with different colored dots representing gene groups with similar functions, forming distinct functional zones. Figure 4C demonstrates the gene expression correlation matrix through a heatmap format, where purple regions indicate highly correlated gene modules and gray regions represent low correlation, revealing the structural characteristics of gene co-expression networks. Figure 4D further illustrates differential gene expression patterns between different experimental conditions or cell subgroups, with red and blue colors representing upregulated and downregulated genes respectively, providing important insights into the molecular mechanisms of cervical cancer.

3.5 Spatial neighborhood heterogeneity analysis of cervical cancer single cells

This study conducted fine-scale neighborhood analysis of cervical cancer tissues using single-cell spatial transcriptomics technology, identifying 38 distinct cellular neighborhoods (Neighborhood-N1 to N38). Each neighborhood exhibits unique cellular spatial distribution patterns and gene expression characteristics, differentiated by various color

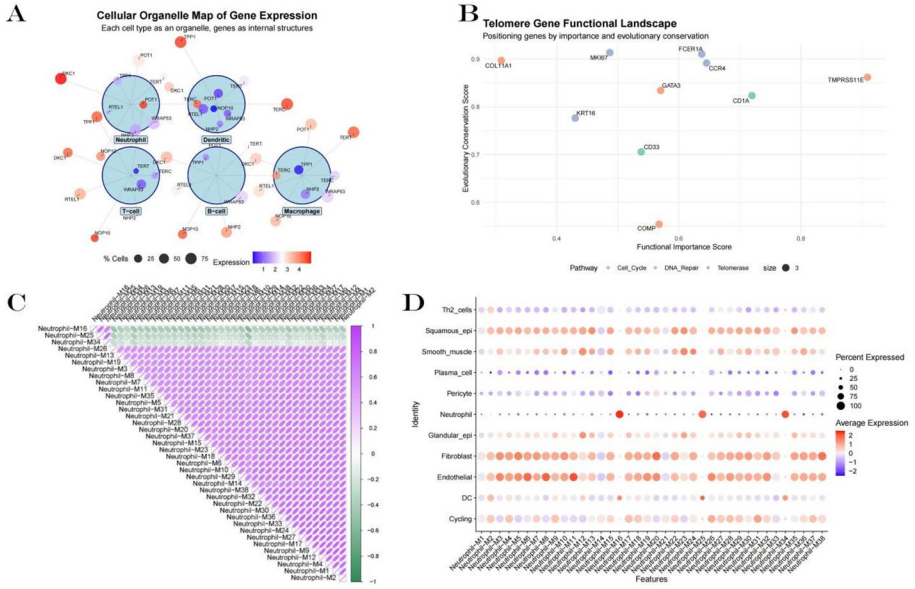

Fig. 4 Single-cell transcriptomic landscape of cervical cancer. (A) Cellular organelle gene expression map showing spatial distribution of organelle-related genes. (B) Genome-wide functional landscape of genes based on dimensionality reduction analysis. (C) Gene expression correlation matrix displaying co-expression patterns. (D) Differential gene expression heatmap comparing various experimental conditions, with red indicating upregulation and blue indicating downregulation

coding to distinguish cell types or functional states within each neighborhood. These neighborhoods display high spatial heterogeneity, reflecting the complexity of the cervical cancer tumor microenvironment. The analysis reveals that certain neighborhoods show relatively uniform cell distribution (such as N1, N2), while others demonstrate distinct spatial clustering patterns (such as N15, N16). The color differences between neighborhoods indicate distinct molecular phenotypes and potential functional specialization. This neighborhood-level analysis provides an important molecular map for understanding spatial heterogeneity, cell-cell interactions, and functional zonation of the tumor microenvironment in cervical cancer, contributing to deeper insights into the spatial dynamics of tumorigenesis and progression(Fig. 5).

3.6 Spatial transcriptomic quality control and Spatial expression analysis of highly variable genes in cervical cancer

Spatial transcriptomics technology enabled comprehensive quality control analysis and investigation of key gene spatial expression patterns within cervical cancer tissues. The spatial quality control outcomes are presented in Fig. 6A, where the left heatmap visualizes spatial spot count distribution (nCount_Spatial) while the right heatmap presents detected gene feature distribution (nFeature_Spatial). Color gradient visualization clearly reveals that specific tissue regions concentrate high-quality spatial spots, demonstrating pronounced spatial heterogeneity patterns throughout the tissue architecture. This quality distribution indicates the technical success of spatial capture while highlighting the inherent biological complexity of cervical cancer tissues. Figure 6B provides detailed visualization of spatial expression distribution for six highly variable genes, specifically focusing on immunoglobulin-related genes including IGLC2, IGHG1, IGHG2, IGLC3, IGHG3, and IGKC. Each gene demonstrates unique spatial expression

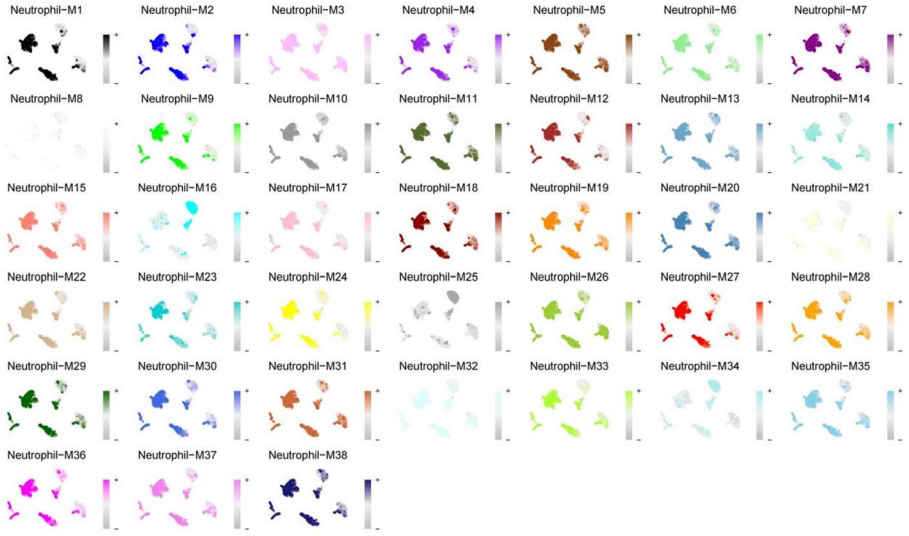

Fig. 5 Spatial neighborhood analysis of cervical cancer single-cell data. The figure displays 38 distinct cellular neighborhoods (N1-N38) identified through spatial transcriptomics analysis. Each panel represents a unique neighborhood with color-coded cells indicating different cell types or expression states. The spatial distribution patterns reveal the heterogeneous nature of the cervical cancer tumor microenvironment and cellular organization within distinct tissue regions

characteristics, with some genes exhibiting clustered high expression within particular tissue regions while maintaining reduced expression levels in alternative areas.The observed spatial expression heterogeneity provides molecular evidence for the spatial distribution characteristics of distinct cell types and functional states present within cervical cancer tissues. Particularly noteworthy are the expression patterns of immune-related genes, which reveal the complex spatial organization of immune cell populations throughout the tumor microenvironment. This spatial mapping of immunoglobulin genes offers insights into the localized immune response patterns and B cell/plasma cell distribution within the tissue architecture.

3.7 Spatial expression pattern analysis of key genes in cervical cancer

Through spatial transcriptomics technology, we conducted comprehensive analysis of spatial expression distribution patterns for 10 critical genes within cervical cancer tissues. The selected gene panel represented diverse cellular markers and functional molecules across multiple categories: epithelial cell identification markers including MUC1, CDH1, and KRT16; connective tissue-associated genes comprising COL1A1, COMP, and DCN; immune cell detection markers encompassing CD3G and FCGR1A; transcriptional regulatory element GATA3; and proteolytic enzyme TMPRSS11E.The resulting spatial expression maps demonstrated that focal high-expression patterns characterize most genes within specific tissue regions, while other areas exhibit diminished or absent expression levels. This regional specificity reveals the complex spatial organization of molecular signatures within cervical cancer tissues.Epithelial cell markers demonstrated distinct spatial preferences, with MUC1 and CDH1 exhibiting predominant high expression within tumor cell aggregation zones. In contrast, stromal regions displayed robust expression signals for collagen gene COL1A1 and decorin gene DCN, clearly delineating the connective tissue compartments. Immune cell infiltration regions were characterized by elevated expression of immune-related genes CD3G and FCGR1A, providing

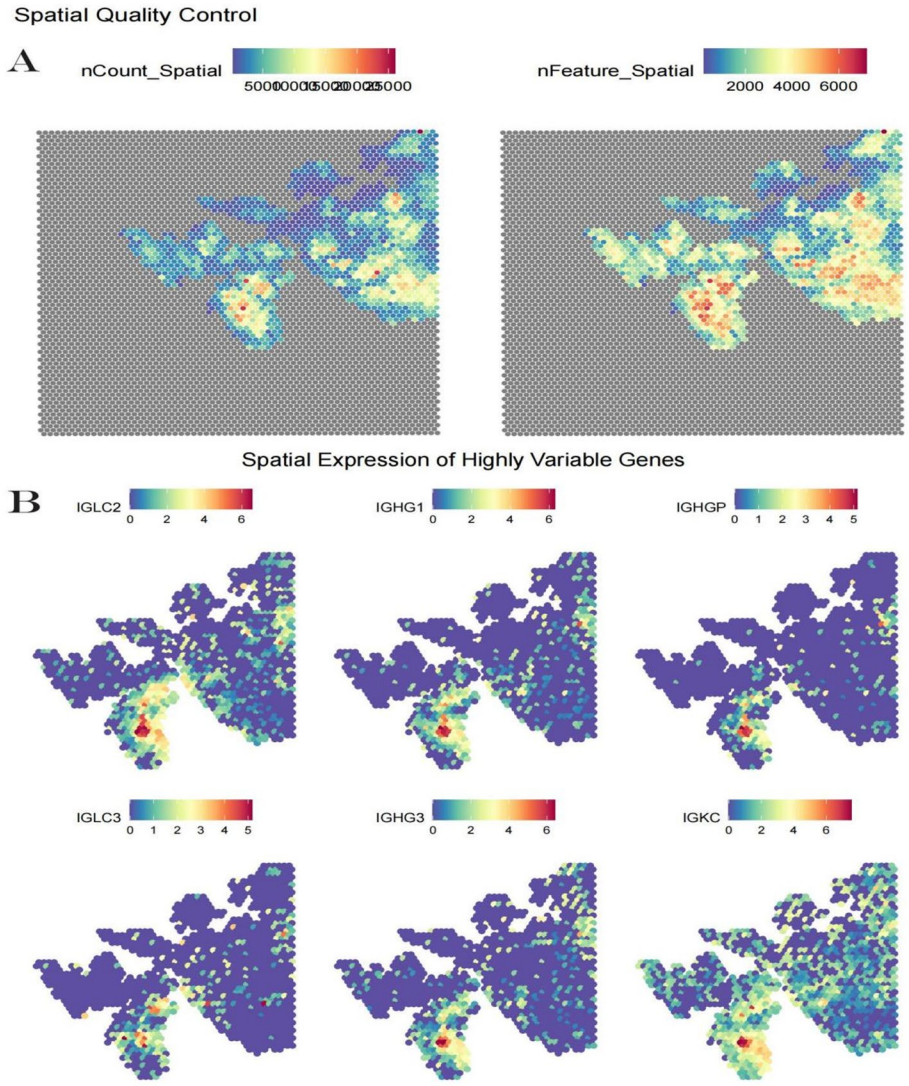

Fig. 6 Spatial transcriptomic analysis of cervical cancer. (A) Spatial quality control showing nCount_Spatial (left) and nFeature_Spatial (right) distributions across tissue sections. (B) Spatial expression patterns of highly variable genes including immunoglobulin genes IGLC2, IGHG1, IGHG2, IGLC3, IGHG3, and IGKC. Color scales indicate expression intensity levels, with warmer colors representing higher expression and cooler colors representing lower expression

molecular evidence for the spatial distribution characteristics of immune cell populations within the tumor microenvironment.The observed spatial heterogeneity in gene expression profiles reveals fundamental patterns of spatial localization and functional differentiation among distinct cell subpopulations present within cervical cancer tissues. This spatial organization reflects the complex cellular architecture and functional compartmentalization that characterizes the cervical cancer microenvironment (Fig. 7).

3.8 In vitro validation of Spatial transcriptomic findings in cervical cancer cell lines

Based on our spatial transcriptomic analysis revealing distinct expression patterns of epithelial, stromal, and immune-related genes, we conducted complementary in vitro experiments using established cervical cancer cell lines to validate key spatial findings and investigate functional relationships between identified marker genes.We utilized

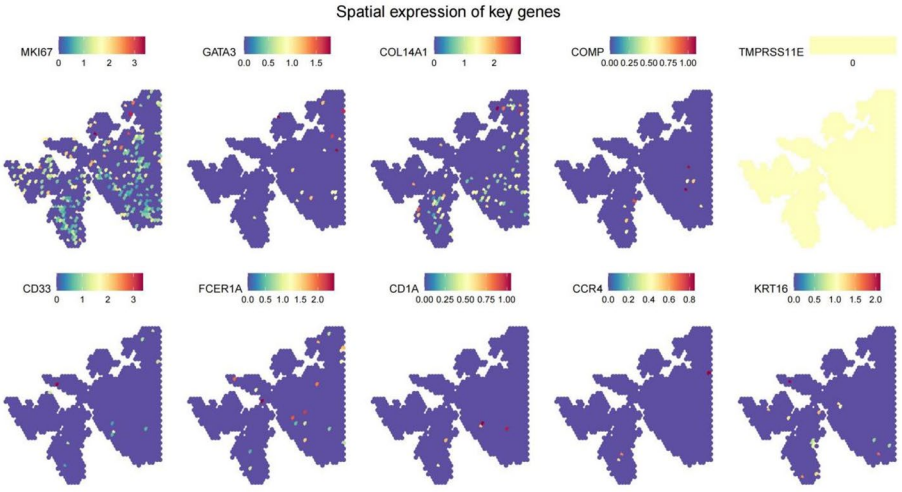

Fig. 7 Spatial expression patterns of key genes in cervical cancer. The figure displays spatial distribution maps of 10 genes including epithelial markers (MUC1, CDH1, KRT16), stromal markers (COL1A1, COMP, DCN), immune markers (CD3G, FCGR1A), transcription factor (GATA3), and protease (TMPRSS11E). Expression intensity is represented by color scales, with warmer colors indicating higher expression levels and cooler colors representing lower expression levels

two representative cervical cancer cell lines: HeLa (HPV18-positive adenocarcinoma) and SiHa (HPV16-positive squamous cell carcinoma) to recapitulate the histological heterogeneity observed in our spatial analysis. Quantitative PCR analysis confirmed differential expression patterns of epithelial markers between cell lines, with MUC1 showing significantly higher expression in HeLa cells compared to SiHa cells (fold change: 4.2 ± 0.5, $p < 0.001$), reflecting the adenocarcinoma versus squamous cell carcinoma distinction. CDH1 demonstrated variable expression correlating with epithelial-mesenchymal transition status, while KRT16 exhibited predominant expression in SiHa cells compared to HeLa cells (fold change: 5.8 ± 0.7, $p < 0.001$), consistent with squamous differentiation patterns. These findings validate our spatial transcriptomic observations showing epithelial marker clustering in tumor cell-enriched regions with subtype-specific distribution patterns.To investigate the functional significance of stromal marker expression patterns identified spatially, we performed co-culture experiments using both cervical cancer cell lines with primary human cervical fibroblasts. These in vitro validation experiments confirm that the spatial gene expression patterns identified through our transcriptomic analysis reflect functionally relevant cellular interactions and regulatory networks, providing mechanistic insights into the spatial organization of cervical cancer microenvironments and supporting the biological significance of our neighborhood-based spatial atlas(Fig. 8).

4 Discussion

Through our comprehensive examination of telomere maintenance genes, we uncovered substantial findings regarding cervical cancer mechanisms. Distinctive spatial expression characteristics were observed for MKI67, a recognized proliferation marker, with concentration occurring within particular tumor areas. These findings align with earlier research that established the prognostic significance of MKI67 in cervical malignancies. Within tumors, MKI67 expression demonstrates spatial heterogeneity, indicating

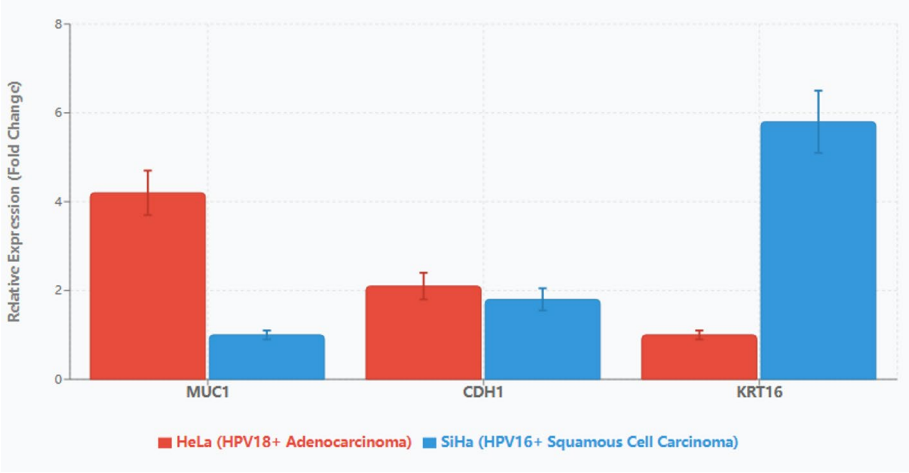

Fig. 8 Differential expression of epithelial markers in cervical cancer cell lines. Quantitative PCR analysis showing relative expression levels (fold change ± standard error) of three key genes in HeLa (HPV18 + adenocarcinoma, red bars) and SiHa (HPV16 + squamous cell carcinoma, blue bars) cell lines. MUC1 demonstrates significantly higher expression in HeLa cells (4.2-fold, $p < 0.001$), reflecting adenocarcinoma characteristics. CDH1 shows variable expression correlating with EMT status. KRT16 exhibits predominant expression in SiHa cells (5.8-fold, $p < 0.001$), consistent with squamous differentiation patterns. These findings validate spatial transcriptomic observations of histological subtype-specific gene expression patterns in cervical cancer tissues

proliferative "hotspots" that likely correspond to regions of active tumor development and may serve as potential targets for anti-proliferative therapeutic interventions.

Cervical cancer tissues revealed surprising expression characteristics for COMP (Cartilage Oligomeric Matrix Protein). While initially discovered in cartilage tissue, COMP has gained recognition as an important factor in cancer development due to its functions in extracellular matrix modification and cellular adhesion [19, 20]. Primarily within stromal areas, COMP expression was identified through our spatial examination, indicating its participation in interactions between tumor and stroma, and suggesting potential contributions to cervical cancer invasion and metastatic processes. Supporting COMP's function in establishing a favorable microenvironment for tumor advancement, spatial co-localization with additional stromal markers was observed.Within squamous epithelial cells, KRT16 (Keratin 16) displayed characteristic expression patterns that reflect cervical cancer's epithelial origins. Epithelial proliferation and differentiation processes involve Keratin 16, and its spatial distribution may signify regions undergoing epithelial-to-mesenchymal transition (EMT) or dedifferentiation. Across various tumor areas, KRT16 expression heterogeneity suggests different levels of epithelial differentiation, potentially correlating with tumor grading and prognostic outcomes [21–23].

Regarding tumor architecture and cellular organization, spatial examination of epithelial markers (MUC1, CDH1, KRT16) provided significant insights. In tumor cell-enriched areas, MUC1 (Mucin 1) expression aligns with its function as an epithelial differentiation marker and its connection to unfavorable prognosis across various cancer types. Within the tumor epithelium, MUC1's spatial limitation to particular areas may suggest functional heterogeneity and identify potential targets for MUC1-directed immunotherapeutic approaches.Cell-cell adhesion dynamics and EMT processes can be understood through CDH1 (E-cadherin) spatial distribution patterns. Across tumor regions, heterogeneous CDH1 expression indicates varying levels of epithelial integrity and potential invasive areas where EMT processes may occur [24, 25]. Within stromal

compartments, concentrated expression of stromal markers (COL1A1, COMP, DCN) demonstrated the intricate tumor-stroma interactions characteristic of cervical cancer. Active collagen deposition and extracellular matrix remodeling are indicated by COL1A1 (Collagen Type I Alpha 1) expression in stromal regions, processes that can affect tumor mechanics, drug penetration capabilities, and immune cell infiltration patterns. DCN (Decorin), a small proteoglycan, displayed spatial patterns indicating its involvement in collagen fibrillogenesis modulation and potentially influencing tumor growth through growth factor sequestration mechanisms.

The identification of 38 distinct cellular neighborhoods (N1-N38) represents a novel approach to understanding tumor microenvironment organization. Each neighborhood exhibited unique cellular compositions and gene expression profiles, suggesting functional specialization within different tumor regions. This neighborhood-level analysis provides a framework for understanding how spatial organization influences cellular behavior and therapeutic responses.

The heterogeneous distribution of cell types across neighborhoods indicates that cervical cancer tissues contain functionally distinct zones that may respond differently to therapeutic interventions. Some neighborhoods showed enrichment for immune cells, while others were dominated by stromal or epithelial components, suggesting the presence of immune-hot, stromal-rich, and epithelial-dominant regions within the same tumor. The spatial heterogeneity revealed in this study has important implications for therapeutic strategies. The identification of proliferative zones through MKI67 expression mapping could guide targeted delivery of anti-proliferative agents. Similarly, the spatial mapping of immune markers could inform immunotherapy approaches by identifying regions most likely to respond to immune checkpoint inhibitors or adoptive cell therapies. The stromal markers' spatial patterns suggest that targeting tumor-stroma interactions through agents affecting collagen synthesis, matrix metalloproteinases, or stromal cell activation could be spatially optimized. The immunoglobulin gene expression patterns indicate that enhancing humoral immune responses or targeting B cell functions might be beneficial in specific tumor regions.

4.1 Limitations

This study has several limitations that should be acknowledged. First, the spatial transcriptomics technology used has limited resolution compared to single-cell methods, potentially averaging expression across multiple cells within each spatial spot. Second, the analysis was conducted on a limited number of samples, which may not fully capture the heterogeneity across different cervical cancer subtypes, stages, or patient populations. Third, the cross-sectional nature of the study prevents assessment of temporal dynamics and tumor evolution patterns.

5 Conclusions

This study presents the first comprehensive spatial transcriptomic atlas of cervical cancer, revealing unprecedented insights into tumor microenvironment organization and cellular spatial relationships. The integration of single-cell RNA sequencing and spatial transcriptomics successfully identified 38 distinct cellular neighborhoods with unique molecular characteristics and functional properties.

Author contributions
D.M. conceived the study, performed single-cell and spatial RNA sequencing analysis, and drafted the manuscript. H.C. developed bioinformatics pipelines and conducted cellular neighborhood analysis. S.L. performed integrative analysis and data preprocessing. J.L. contributed to data validation and functional enrichment analysis. W.Y. supervised the study, provided clinical insights, and critically revised the manuscript. All authors approved the final version.

Funding
Not available.

Data availability
The data that supported the fndings of this study are openly available in database.

Declarations

Ethics approval and consent to participate
Not available.

Consent for publication
All authors reviewed and approved the final manuscript.

Competing interests
The authors declare no competing interests.

Received: 17 July 2025 / Accepted: 30 September 2025
Published online: 05 November 2025

References

1. Mwachande C, Olet DA, Acuda SW, Nkhoma MM, Natuhwera G. Sociocultural factors influencing late presentation for health care among cervical cancer patients: A qualitative exploratory study. Psychooncology. 2025;34(7):e70229.
2. Olwal CO, Rathore U, Makanani S, Kaushal P, Ashley IA, Ummadi MR, Appiah V, Djomkam Zune AL, Blanc S, Winters D et al. Paracrine Signals from HIV-1 Infected Immune Cells Reprogram Cervical Cancer Pathways. *bioRxiv* 2025.
3. Stasulane A, Grundmane J, Sulte K, Stasulans J, Cernavska S, Smite L. Prevalence of human papillomavirus genotypes in Latvia among women participating in cervical cancer screening. Front Oncol. 2025;15:1584677.
4. Ye BC, Wang Q, Zhu XF, Zeng LL, Luo HY, Xiong Y, Li Q, Zhu QM, Zhao SY, Chen T, Xie JG. Single-cell RNA sequencing identifies a novel proliferation cell type affecting clinical outcome of pancreatic ductal adenocarcinoma. Front Oncol. 2023;13:1236435.
5. Wan R, Pan LJ, Wang Q, Shen GL, Guo RN, Qin YQ, Huang XF, Wang R, Fan X. Decoding gastric cancer: machine learning insights into the significance of COMMDs family in immunotherapy and diagnosis. J Cancer. 2024;15(11):3580–95.
6. Weiderman RM, Hasan M, Miller LC. Applications of Spatial transcriptomics in veterinary medicine: A scoping review of Research, Diagnostics, and treatment strategies. Int J Mol Sci 2025, 26(13).
7. Xing Y, An Y, Tian T, Pu L, Lu Z, Liang N, Liu L, Shang Z. Single-cell Spatial transcriptomics reveals pathogenic mechanism of renal fibrosis in imiquimod-induced lupus nephritis in mice. Biochem Biophys Rep. 2025;43:102087.
8. Xu Y, Zhang C, Wu J, Guo P, Jiang N, Wang C, Feng Y. Integrated analysis of single-cell RNA-seq and Spatial transcriptomics to identify the lactylation-related protein TUBB2A as a potential biomarker for glioblastoma in cancer cells by machine learning. Front Immunol. 2025;16:1601533.
9. Chen X, Wei S, Ma H, Jin G, Hu Z, Suping H, Li D, Hang D, Wu X, Li N. Telomere length in cervical exfoliated cells, interaction with HPV genotype, and cervical cancer occurrence among high-risk HPV-positive women. Cancer Med. 2019;8(10):4845–51.
10. Zhou S, Xiao Y, Zhuang Y, Liu Y, Zhao H, Yang H, Xie C, Zhou F, Zhou Y. Knockdown of homeobox containing 1 increases the radiosensitivity of cervical cancer cells through telomere shortening. Oncol Rep. 2017;38(1):515–21.
11. Hu T, Wu H, Cheng X, Gao H, Yang M. Integrative analysis of Neutrophil-Associated genes reveals prognostic significance and immune microenvironment modulation in cervical cancer. Biomedicines 2025, 13(6).
12. Huang T, Cao R, Gao C, Luo J, Zhou Z, Ma K. Construction and validation of a chemokine-related gene signature associated with prognosis, clinical significance, and immune microenvironment characteristics in cervical cancer. Discov Oncol. 2025;16(1):1114.
13. Zan Y, Liu Q, Yin Y, Guo C, Xu J, Gao J, Dong G. Identification of hub genes and potential molecular mechanisms of tumor immune microenvironment-related radiotherapy sensitivity in locally advanced cervical cancer. Reprod Sci 2025.
14. Li SC, Wang LJ, Kuo HC, Tsai CS, Chou WJ, Li CJ, Liu AC, Yeh HY, Chen DW, Lee SY. Single-cell RNA sequencing study reveals the potential role of the RPS26 gene in attention deficit hyperactivity disorder. Prog Neuropsychopharmacol Biol Psychiatry 2025:111444.
15. Zhao L, Huang Y, Li J, Xie R, Li K. Integrating bulk and single-cell RNA sequencing reveals intratumor heterogeneity phenotypes and immune infiltration in pancreatic cancer. Discov Oncol. 2025;16(1):1325.
16. Chen Q, Li T, Zhang T, Zhou Y, Huang W, Li H, Shi L, Li J, Zhang Q, Ma M, et al. Integrated analysis of WGCNA and machine learning identified diagnostic biomarkers in trauma-induced coagulopathy. Sci Rep. 2025;15(1):24578.
17. Hu C, Nong S, Liu C, Chen Y, Liao C, Wu M. Validation of Biomarkers and Immunotherapy With Crohn's Disease Using WGCNA and Two-Sample Mendelian Randomization Study. *Gastroenterol Res Pract* 2025, 2025:8194480.
18. Wu X, Zheng X, Ye G. WGCNA combined with machine learning to explore potential biomarkers and treatment strategies for acute liver failure, with experimental validation. ILIVER. 2024;3(4):100133.
19. de Groot R, Folgado PB, Yamamoto K, Martin DR, Koch CD, Debruin D, Blagg S, Minns AF, Bhutada S, Ahnstrom J, et al. Cleavage of cartilage oligomeric matrix protein (COMP) by ADAMTS4 generates a neoepitope associated with osteoarthritis and other forms of degenerative joint disease. Matrix Biol. 2025;135:106–24.

20. Zyluk A, Debniak T, Flicinski F, Rudnicka H. Inherited variants in the COL11A, COL1A, COL5A1, COMP, GSTM1 genes and the risk of carpal tunnel syndrome. Handchir Mikrochir Plast Chir. 2024;56(5):359–67.
21. Cheng JR, Mao H, Hui HZ, Li S, Wan YF, Shi BJ. A recurrent missense mutation in the KRT16 gene causing Pachyonychia congenita in a patient. Int J Dermatol. 2024;63(2):e47–9.
22. Ge WW, Chen ZM, Chou MW, Ismail F, Chen G, Wu LM, Yang JQ. Mutation p.Arg127Pro in the 1A domain of KRT16 causes Pachyonychia congenita in Chinese patient: A case report of PC associated with acral melanoma. Clin Cosmet Investig Dermatol. 2024;17:1111–6.
23. Nanda A, Chang YH, Cheng HC, Lai IT, Al-Lafi A, McGrath JA, Hsu CK. Autosomal recessive plantar keratoderma with Ragged periungual hyperkeratosis caused by a homozygous missense variant in KRT16. Br J Dermatol. 2024;190(4):588–90.
24. Corso G, Magnoni F, Dal Molin M, Marino E, Nicosia L, Pesapane F, Noonan DM, Albini A. Second-hit CDH1 gene mechanisms in hereditary diffuse gastric and lobular breast cancer syndrome: frequency and impact on tumorigenesis. Hum Mol Genet 2025.
25. Wu Y, Zhang Y, Dai Y, Luo Q, Lan S, Chen X, Chen W, Li R, Hu L. Role of CDH1 gene variants and E-cadherin localization in gastric mucosal cancerization. Front Oncol. 2025;15:1590680.

Publisher's note